Computer Vision and Image Understanding 113 (2009) 202–211

Contents lists available at ScienceDirect

Computer Vision and Image Understanding

journal homepage: www.elsevier.com/locate/cviu

3D reconstruction of a femoral shape using a parametric model and two 2D fluoroscopic images

Ryo Kurazume [a,*], Kaori Nakamura [a], Toshiyuki Okada [b], Yoshinobu Sato [c], Nobuhiko Sugano [c], Tsuyoshi Koyama [d], Yumi Iwashita [a], Tsutomu Hasegawa [a]

[a] Graduate School of Information Science and Electrical Engineering, Kyushu University, 744 Motooka, Nishi-ku, Fukuoka 819-0395, Japan
[b] Osaka University Hospital, Medical Center for Translational Research, 2-15 Yamadaoka, Suita-shi, Osaka 565-0871, Japan
[c] Graduate School of Medicine, Osaka University, 2–2 Yamadaoka, Suita-shi, Osaka, 565-0871, Japan
[d] Department of Orthopaedic Surgery, National Hospital Organization Osaka-Minami Medical Center, 2-1 Kidohigashimachi, Kawachinagano, Osaka 586-8521, Japan

ARTICLE INFO

Article history:
Received 18 September 2007
Accepted 15 August 2008
Available online 12 September 2008

Keywords:
Fluoroscopic image
Parametric femoral model
Registration
Medical image diagnosis

ABSTRACT

In medical diagnostic imaging, the X-ray CT scanner and the MRI system have been widely used to examine 3D shapes and internal structures of living organisms and bones. However, these apparatuses are generally large and very expensive. Since an appointment is also required before examination, these systems are not suitable for urgent fracture diagnosis in emergency treatment. However, X-ray/fluoroscopy has been widely used as traditional medical diagnosis. Therefore, the realization of the reconstruction of precise 3D shapes of living organisms or bones from a few conventional 2D fluoroscopic images might be very useful in practice, in terms of cost, labor, and radiation exposure. The present paper proposes a method by which to estimate a patient-specific 3D shape of a femur from only two fluoroscopic images using a parametric femoral model. First, we develop a parametric femoral model by the statistical analysis of 3D femoral shapes created from CT images of 56 patients. Then, the position and shape parameters of the parametric model are estimated from two 2D fluoroscopic images using a distance map constructed by the Level Set Method. Experiments using synthesized images, fluoroscopic images of a phantom femur, and in vivo images for hip prosthesis patients are successfully carried out, and it is verified that the proposed system has practical applications.

1. Introduction

In medical diagnostic imaging, the X-ray Computed Tomography (CT) scanner and the Magnetic Resonance Imaging (MRI) system have been widely used to examine the 3D shape or internal structure of living organisms and bones. However, these apparatuses are generally large and very expensive, and thus, they are usually installed in large medical institutions rather than small local clinics. Since an appointment is also required before examination, these systems are not suitable for urgent fracture diagnosis in emergency treatment.

Meanwhile, X-ray/fluoroscopy has been widely used as traditional medical diagnosis. Recently, digital fluoroscopy has been developed and widely used in many hospitals. The cost of this fluoroscopic inspection system is much lower than that of CT or MRI systems and the system can be dealt with more conveniently. Furthermore, the risk of radiation exposure is also lower than that of the CT inspection system.

From the above considerations, the realization of the reconstruction of precise 3D shapes of living organisms or bones from a few conventional 2D fluoroscopic images might be very useful in practice, in terms of cost, labor, and radiation exposure. In particular, there is a strong demand from surgeons for 3D computer-aided surgery without laborious CT imaging for simple surgeries such as artificial joint replacement or fracture treatment. A practical 3D diagnostic system using common 2D fluoroscopic images is desired.

However, 3D shape reconstruction from a 2D image is a fundamentally ill-posed problem, and so a sufficient number of images must be obtained, or several constraint conditions for the 3D shape must be determined. However, the shapes of bones have inherent and universal patterns, and thus, by modelling such inherent patterns, 3D shape reconstruction from a few 2D images is possible.

In the present paper, a technique by which to estimate the patient-specific 3D shape of a femur from only two fluoroscopic images is proposed. The proposed technique utilizes a parametric femoral model constructed by statistical analysis of 3D femoral shapes created from CT images of 56 patients. The position/orientation and shape parameters of the parametric model are then estimated from two 2D fluoroscopic images by solving the 2D/3D registration problem using a distance map constructed by the Level Set Method.

The 2D/3D registration problem is well established in image processing, especially for texture mapping in Computer Graphics

* Corresponding author. Fax: +81 92 802 3607.
E-mail address: kurazume@is.kyushu-u.ac.jp (R. Kurazume).

1077-3142/$ - see front matter © 2008 Elsevier Inc. All rights reserved.
doi:10.1016/j.cviu.2008.08.012

or Augmented Reality. For a rigid object, (1) feature-based techniques [1–3], (2) image-based techniques using texture, reflectance, brightness, and shading [4,5,6], and (3) silhouette-based techniques [7–10], have been proposed. In particular, in surgical navigation systems, Digitally Reconstructed Radiographs (DRRs) [11,12] are widely used in 2D/3D registration for the fluoroscopy-guided surgery. However, the construction of DRR is time-consuming and special techniques such as the use of graphics hardwares is indispensable for quick medical diagnosis. Since texture or shadow are usually unavailable in fluoroscopic images, fast 2D/3D registration technique using simple and robust features such as silhouette and contour lines is desirable.

In 2D/3D registration of a non-rigid object such as soft tissues in medical imaging, similarity measure [13,14], mutual information [15], affine [16,17], geometric hashing [18], and displacement-field-based transformation [19] have been proposed and tested. In addition, the 3D shape estimation of a parameterized object, such as the shape reconstruction of mathematical plaster models with unknown parameters using a laser range finder [20], or the comparison of multiple cross-section images of a 3D model and a 3D parametric model [21], has also been studied. However, these studies assumed the use of a sufficient number of images or a precise 3D shape taken by a laser range finder, and only a few studies have examined 3D non-rigid shape reconstruction from only a few 2D images [22–24]. Zheng et al. [24] proposed a similar approach with our method for estimating a femoral shape from fluoroscopic images. Their technique is based on an active shape model and conventional ICP method. They introduced experiments for 11 cadaveric femurs using three fluoroscopic images including the one taken from the longitudinal direction of the femoral shaft. However, detailed discussion using in vivo images taken by clinical setting and calibration technique for fluoroscopic imaging was not presented.

This paper propose the 3D reconstruction technique of a femoral shape using two in vivo fluoroscopic images of patients. A distance map constructed by the Level Set Method is utilized for fast and robust 2D/3D registration with M-estimator. The calibration technique for fluoroscopic imaging using two kinds of calibration markers is also presented. This paper is organized as follows. Section 2 describes the statistical shape model of the femur proposed by Okada, et al. [25,26] at first. Then, we introduces the proposed 3D reconstruction technique of a femoral shape using the statistical shape model and two 2D fluoroscopic images. In Section 3, experiments using synthesized images, fluoroscopic images of a phantom femur, and in vivo images for hip prosthesis patients, are successfully carried out, and it is verified that the proposed system has practical applications. Finally, Section 4 presents our conclusion.

2. 3D parametric femoral model

In this section, we introduce the 3D reconstruction technique of a femoral shape using the statistical shape model and two 2D fluoroscopic images.

2.1. Overview of the proposed algorithm

The procedure of the proposed technique is summarized as follows:

(1) First, we develop a 3D parametric femoral model by the statistical analysis of 3D femoral shapes created from CT images of 56 patients. With this model, a general 3D shape of the femur is expressed by the average shape and several shape parameters. Thus, the 3D shape estimation of the patient's femur from two 2D fluoroscopic images can be divided into two procedures, the determination of optimum position and orientation of the 3D model in two 2D fluoroscopic images (Step 2) and the estimation of optimum shape parameters (Step 3).
(2) The position and orientation of the parametric model in two 2D fluoroscopic images are determined by the 2D/3D registration technique using a distance map constructed by the Level Set Method.
(3) The optimum shape parameters of the parametric model are estimated by comparing the silhouette contour of the parametric model and two 2D fluoroscopic images using a distance map obtained in Step 2.
(4) Step 2 and 3 are repeated until the residual error between the silhouette contour of the parametric shape model and two 2D fluoroscopic images becomes less than a threshold value.

Each of the above steps is explained in details in the following sections.

2.2. 3D parametric femoral model

We utilize the statistical shape model of the femur proposed by Okada et al. [25,26]. In this technique, a number of 3D femoral shapes created from CT images are analyzed statistically, and the parametric femoral model [27,28], which consists of the average 3D shape and several shape parameters, is created. With this parametric femoral model, a general 3D shape of the femur is expressed by the average shape and several shape parameters.

The concrete procedure for creating a parametric 3D femoral model is as follows:

1. Surface models of femurs are created from CT images by manual segmentation and Marching Cubes.
2. Local coordinate axes of the surface models are determined by applying the principal component analysis (PCA) to the set of 3D positions of the node points in each surface model. The center of gravity is defined as the origin of the local coordinate system. The Z axis is determined as the axis corresponding to the largest eigenvalue, which is toward the longitudinal direction of the femoral shaft from the hip to knee. The region up to 35% of total length of the femur along the Z axis from the femoral head top defined as the node point having the minimum Z coordinate is extracted as a proximal femur, where the total length is defined as the difference of the maximum and minimum Z coordinates in the femur surface model, and the value of 35% is determined so as to cover a region anatomically regarded as a proximal femur.
3. One of the femoral model is selected as the reference model and displacement vector fields to all other models described by the thin-plate spline are calculated using a point-based non-rigid registration algorithm[29]. Although the approximation accuracy of the resulted parametric model may somewhat depend on the selected reference model, we currently selected it based on visual assessment so that it is not largely deviated from the average shape.The reference model is decimated using an algorithm available in the visualization toolkit so that the number of nodes of the surface model becomes 1500. 1500 points were used because the proximal femur shape can be represented in a reasonable accuracy using 1500 points while computational cost for the non-rigid registration is still acceptable, for example, less than 10 min for each case.The reference model is non-rigidly registered with each of other models so as to find the corresponding 1500 points on each model. The non-rigid registration algorithm [29] generate 3D displacement vector

field from the reference to each dataset. The 1500 points of each model are determined by combining those of the reference model and the generated displacement vector field. These processes do not guarantee physically-meaningful correspondences. Using these correspondences, however, each surface model can be represented as a 1500×3 dimensional shape vector, that is, a fixed-dimensional vector. For our current purpose, correspondences are acceptable if they are plausible even though there is not some guarantee.

4. Given n shape vectors, the average shape vector is given by their average. PCA is applied to a set of the shape vectors subtracted by the average shape vector to obtain the eigenvectors whose coefficients correspond to the shape parameters.

The parametric femoral model used in the following experiments was created using CT images of 56 patients. By applying PCA to 56 samples of 3D femoral shapes, we extracted the most significant 50 principal components $(p_1, p_2, \ldots, p_{50})$, standard deviation $(\sigma_1, \sigma_2, \ldots, \sigma_{50})$, and corresponding principal vectors $(v_1, v_2, \ldots, v_{50})$. With the obtained parametric femoral model, the general 3D shape of a femur is expressed as

$$x' = x + (p_1 \cdot \sigma_1 \cdot v_1) + (p_2 \cdot \sigma_2 \cdot v_2) + \cdots \quad (1)$$

where x is the surface point of the average shape and x' is the surface point of the general shape. Therefore, the general 3D shape of a femur is expressed by the parametric femoral model with

- average 3D shape and several principal vectors (predetermined)
- several (up to 50) shape parameters (estimated)

Fig. 1 shows the contribution ratio of the shape parameters for the statistical femoral model.

2.3. Reconstruction of 3D femoral shape from two 2D fluoroscopic images

In this section, we introduce the 2D/3D registration algorithm and the estimation procedure of the optimum shape parameters using two fluoroscopic images.

This 2D/3D registration algorithm utilizes the contour lines of the silhouette of the 2D image and the projected contour lines of the 3D model. The optimum position of the 3D model is determined such that the contour lines coincide with each other on the 2D image plane. In commonly used approaches such as the ICP algorithm, the error metric is usually defined as the sum of the distances between the points on the 2D contour lines and their nearest points on the projected contour lines of the 3D model. However, the nearest point search is a laborious task and is time consuming even for the kd tree-based algorithm [30].

In the present approach, the 2D distance map [7] is utilized. First, the 2D distance map from the contour lines is created on the 2D image using the Fast Marching Method [31,32] or raster scan algorithms using local operators [33,34]. Once the 2D distance map is created, the error metric is obtained directly from the 2D distance map as the value at the points on the projected contour lines of the 3D model. Using the course-to-fine strategy called "Distance Band" [7], a 2D distance map can be constructed quite rapidly using the Fast Marching Method.

When 2D/3D registration and estimation of the shape parameters are performed at the same time, the depth from the view point and the scale of the 3D model cannot be distinguished. Therefore, the proposed algorithm utilizes two fluoroscopic images taken from two viewpoints at different positions. In addition, we assume that the 3D femoral parametric model is constituted by a large number of small triangle patches of approximately the same size.

In the following sections, we explain Step 2 and Step 3 shown in Section 2.1. In both steps, 2D distance maps from the extracted contour lines of patient's femur in fluoroscopic images are created at first. Then the error between the contour lines of the femur and the projected contour lines of the 3D model is minimized by reading the distance values of the 2D distance maps.

2.3.1. Registration of 2D fluoroscopic images and the 3D parametric model

A brief description of the registration procedure of the 2D fluoroscopic images and the 3D parametric model is given as follows:

1. Extract the contour lines of the femur in the fluoroscopic images using an active contour model such as snakes or the Level Set Method [31].
2. Construct a 2D distance map from the extracted contour lines using the Fast Marching Method [31,32]. Fig. 2 shows an example of the constructed 2D distance map of a femoral image.
3. Place the parametric femoral model at an arbitrary initial position which is determined manually and calculate the 2D projection image of the 3D model.
4. Extract contour lines of the projected image and corresponding 3D patches of the 3D model. This procedure can be executed quite rapidly by the OpenGL hardware accelerator (Appendix A.1).

5(a). Apply the force calculated from the 2D distance map at the projected contour points directly to the corresponding 3D patch. Details are presented in Section 2.4.

6(a). Using the robust M-estimator, which is a robust estimation technique, the total force and moment around the center of gravity (COG) is calculated.

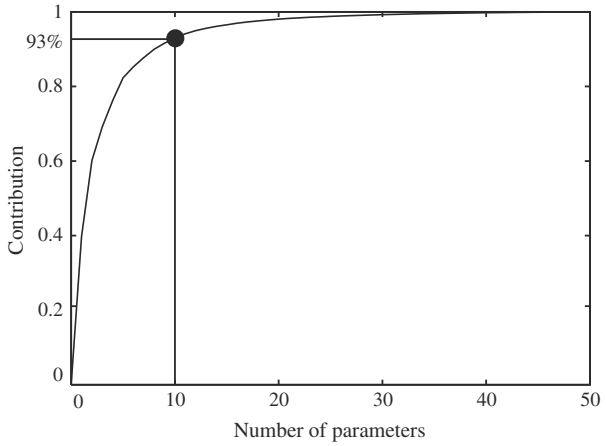

Fig. 1. Contribution of parametric model.

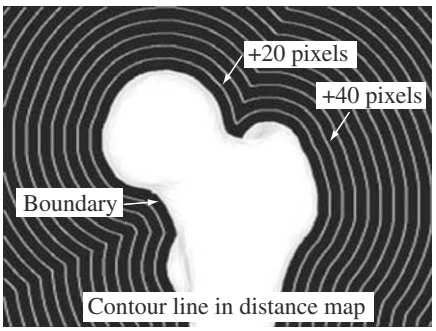

Fig. 2. 2D distance map from contour in the femoral image.

7(a). Steps 3 to 6(a) of the procedure are repeated for two images captured from the different viewpoints sequentially, and the total force and moment are calculated.
8(a). Update the position of the 3D parametric model according to the total force and moment.
9(a). Repeat Steps 3 to 8(a) until the magnitude of the total force and moment becomes less than the pre-defined threshold value.

2.3.2. Estimation of the optimum shape parameters

The estimation procedure of the optimum shape parameters of the 3D parametric femoral model is shown in this section. This procedure also uses the 2D distance map from the contour line of the femur in the fluoroscopic image, which has already been constructed, as described in Section 2.3.1. Therefore, from Steps 1 to 4 are same as Section 2.3.1 and we can skip these procedures by using the obtained 2D distance map in Step 4 of the above procedure, After Step 4, the optimum shape parameters are estimated as follows:

5(b). Calculate the error E, which is defined as the sum of the values of the 2D distance map at the projected contour line of the 3D parametric model.
6(b). Find the optimum shape parameters that minimize the error E at the current position using the conjugate gradient method.
7(b). Reconstruct the 3D shape according the obtained shape parameters using Eq. (1).
8(b). Repeat Steps 3 to 7(b) until the error E becomes less than the pre-defined threshold value.

2.4. 2D/3D registration using the robust M-estimator

After obtaining the distance map on the 2D fluoroscopic image and the list of the triangular patches of the 3D model corresponding to the contour points, the force $\boldsymbol{f}_i$ is applied to all of the triangular patches of the contour points (Figs. 3 and 4), as explained in Step 5(a).

$$\boldsymbol{f}_i = D_i \frac{\nabla D_i}{|\nabla D_i|} \tag{2}$$

where D_i is the value of the distance map at the contour point, which corresponds to the triangular patch i, and ∇D_i is the gradient of D_i.

In Step 6(a), the total force and moment around the center of gravity (COG) is calculated by the following equations:

$$\boldsymbol{F} = \sum_i \psi(\boldsymbol{f}_i) \tag{3}$$

$$\boldsymbol{M} = \sum_i \psi(\boldsymbol{r}_i \times \boldsymbol{f}_i) \tag{4}$$

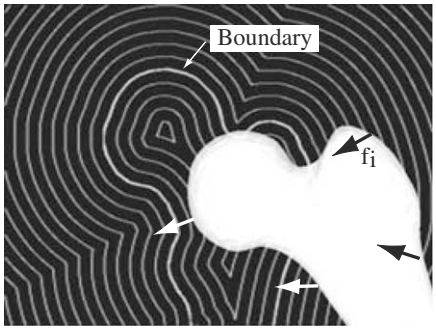

Fig. 3. Force f_i is applied to 3D triangular patch i on the contour line.

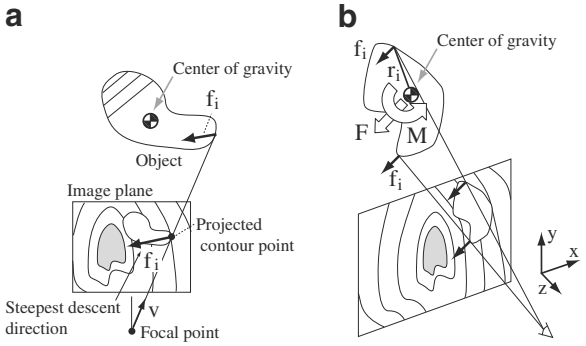

Fig. 4. Calculation of the total force and moment around the center of gravity (COG).

where $\boldsymbol{r}_i$ is a vector from the COG to triangular patch i and $\psi(\boldsymbol{z})$ is a particular estimate function. In practical situations, the contour of the femur is occasionally occluded or blurred, or the 2D image is corrupted by noise. In such cases, the obtained boundary does not coincide with the projected contour of the 3D model and the correct distance value cannot be obtained. To deal with this problem, we introduce the robust M-estimator in order to disregard contour points with large errors. In our implementation, we utilized a following function using a Lorentzian function with a variance σ^2 and a vector $\boldsymbol{z}$.

$$\psi(\boldsymbol{z}) = \frac{1}{1+|\boldsymbol{z}|^2/\sigma^2}\boldsymbol{z} \tag{5}$$

Let us consider the force $\boldsymbol{f}_i$ and the moment $\boldsymbol{r}_i \times \boldsymbol{f}_i$ as an error $\boldsymbol{z}_i$ and the sum of the error as

$$E(\boldsymbol{P}) = \sum_i \rho(\boldsymbol{z}_i) \tag{6}$$

where $E(\boldsymbol{P})$ is a scalar function of a vector $\boldsymbol{P}$ which is the position of the 3D parametric model, and $\rho(\boldsymbol{z})$ is a particular estimate function, which is defined as

$$\frac{\partial \rho(\boldsymbol{z})}{\partial \boldsymbol{z}} = \psi(\boldsymbol{z}) \tag{7}$$

The position $\boldsymbol{P}$ that minimizes the error $E(\boldsymbol{P})$ is obtained as the following equation:

$$\frac{\partial E}{\partial \boldsymbol{P}} = \sum_i \frac{\partial \rho(\boldsymbol{z}_i)}{\partial \boldsymbol{z}_i}\frac{\partial \boldsymbol{z}_i}{\partial \boldsymbol{P}} = \boldsymbol{0} \tag{8}$$

Here, we define the weight function $w(\boldsymbol{z})$ as the following equation in order to evaluate the error term:

$$w(\boldsymbol{z})\boldsymbol{z} = \psi(\boldsymbol{z}) = \frac{\partial \rho(\boldsymbol{z})}{\partial \boldsymbol{z}} \tag{9}$$

From the above equation, we obtain the following weighted least squares method:

$$\frac{\partial E}{\partial \boldsymbol{P}} = \sum_i w(\boldsymbol{z}_i)\boldsymbol{z}_i \frac{\partial \boldsymbol{z}_i}{\partial \boldsymbol{P}} = \boldsymbol{0} \tag{10}$$

In our implementation, the optimum position, which minimizes the error $E(\boldsymbol{P})$, is obtained by the steepest gradient method, as shown in Step 9(a).

3. Experiments

3.1. Simulation using DRRs

First, we conducted the experiments using Digitally Reconstructed Radiographs (DRRs) in order to evaluate the fundamental

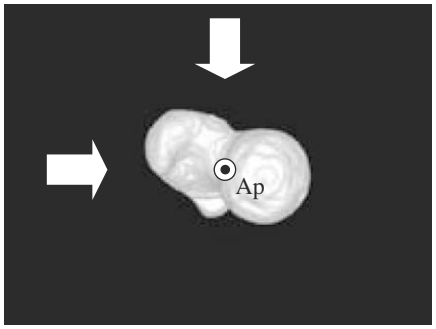

Fig. 5. Directions of DRRs for simulation.

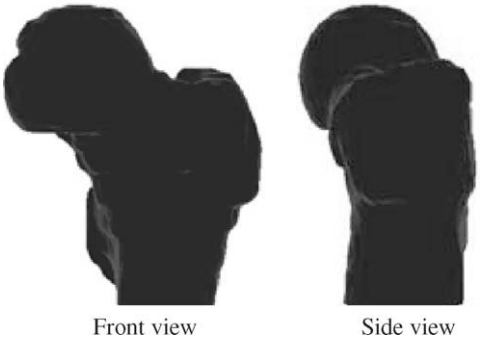

Fig. 6. Examples of DRRs for simulation experiments.

performance of the proposed method. In the experiment, the estimation accuracy for 10 femoral models is examined using two reconstructed fluoroscopic images. Among 10 models, five models (model data 1–5) are used for the construction of the 3D parametric model and five models (test data 1–5) are not used.

We determine the directions of the fluoroscopic images as shown in Fig. 5 considering the possible direction in actual radiographic examination. Under this condition, two view directions meet at right angles at the main axis of the femur A_P. Examples of the reconstructed fluoroscopic images are shown in Fig. 6.

All of the 3D femoral shapes used in the experiments were reconstructed precisely by the CT scanner beforehand, and the optimized shape parameters, which minimize the distance errors between surface points, were determined by comparing the 3D actual shape and the 3D parametric model and searching all possible candidates.

First, we chose up to 10 principal components and estimated the position and optimum shape parameters of the femur on the fluoroscopic images. In this experiment, the position estimation of the femur and the optimum parameter estimation were repeated alternately and independently. An example of the experimental results for test data 4 is shown in Fig. 7, which illustrates the average shape, the actual shape, and the estimated shape.

Fig. 8 indicates the average error between the estimated shape and the actual shape. The average error is defined as the average of the minimum distance from the surface point of the estimated shape to the triangle patches of the actual shape. In this figure, "AS" on the horizontal axis indicates the average error when the position is estimated but all of the shape parameters are fixed to their initial values (all of the parameters are set to "0"). This figure shows that the average error gradually decreases as the number of estimated shape parameters increases. However, the average error converges when the number of shape parameters is approximately five and no significant difference is observed, even if the number of the shape parameters increases.

In addition, Fig. 9 shows the types of errors defined below when the number of estimated shape parameters is five. Table 1 also indicates the average of the error, the standard deviation, the maximum value, and the minimum value for the 10 models.

Average error 1 The average error between the average model and the actual shape.
Average error 2 The average error between the 3D optimized estimated shape and the 3D actual shape obtained by comparing the actual shape and the parametric model.
Average error 3 The average error between the estimated shape and the actual shape obtained by comparing the two 2D fluoroscopic images and the 3D parametric model (proposed method).

The experimental results show that Average error 3 between the estimated shape and the actual shape is less than 1.1 mm at

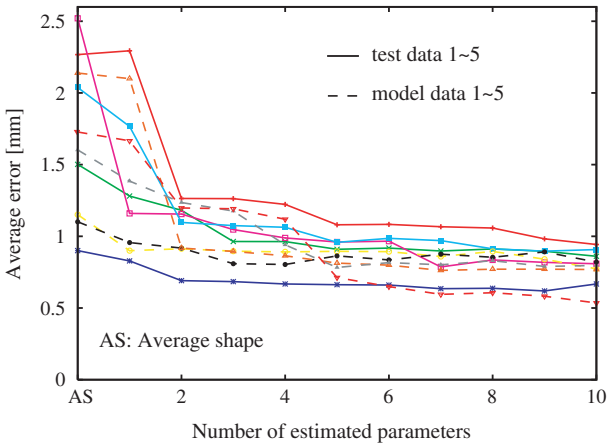

Fig. 8. Average error and number of estimated shape parameters.

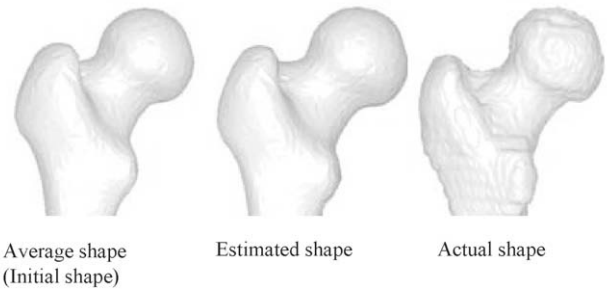

Fig. 7. Actual and estimated femoral model with and without shape parameter estimation.

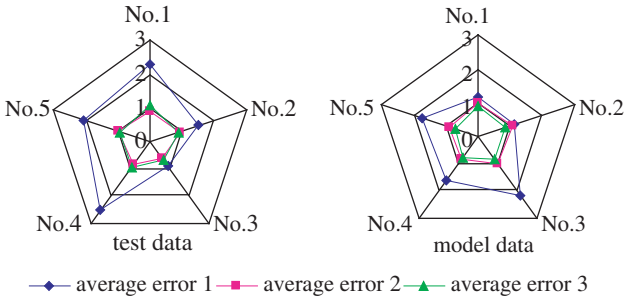

Fig. 9. Average error after shape parameter estimation (number of principal components: 5).

Table 1
Comparison of average errors (mm)

	Average	STD.	Maximum	Minimum
Average error 1	1.69	0.54	2.52	0.90
Average error 2	0.90	0.13	1.06	0.60
Average error 3				
(Test data)	0.91	0.15	1.08	0.66
(Model data)	0.81	0.07	0.90	0.71

worst, and it is verified that the 3D shape can be estimated using two 2D fluoroscopic images with the same accuracy in case that the 3D shapes are compared directly. Moreover, it is confirmed that there is no significant difference between the models that were used for the construction of the parametric femoral model and those that were not.

Note that in some cases in Fig. 9, Average error 3 is smaller than Average error 2. In the calculation of Average error 2, the origin and the direction of the local coordinate systems of the estimated and actual shapes coincide with each other and relative position of these shapes is fixed. On the other hand, for Average error 3, relative position of these shapes is also optimized by 2D/3D registration proposed in Section 2.3, and Average error 3 becomes smaller than Average error 2.

3.2. Experiments using the phantom femur

We conducted experiments using a dry femur bone and fluoroscopic images. In these experiments, a special fluoroscopic imaging apparatus (Siemens, Siremobil ISO-C) was used for the fluoroscopic photography from various directions around the phantom femur.

First, we captured images of calibration markers with nine glass bubbles (left of Fig. 10) at 50 positions around the markers from 0 to 190° using the fluoroscopic apparatus. The 3D positions of the markers were also measured precisely by the CT scanner. Next, the intrinsic and extrinsic parameters of the fluoroscopic apparatus were calibrated by Tsai's method [35].

After calibration, we replaced the markers with the dry femur bone and captured 50 images at the same positions. In addition, the precise 3D shape of the dry bone was measured by the CT scanner. Next, we chose two fluoroscopic images from 50 images, as mentioned below, and estimated the position and the optimum parameters in fluoroscopic images using the proposed techniques. Examples of the fluoroscopic images are shown in Fig. 11.

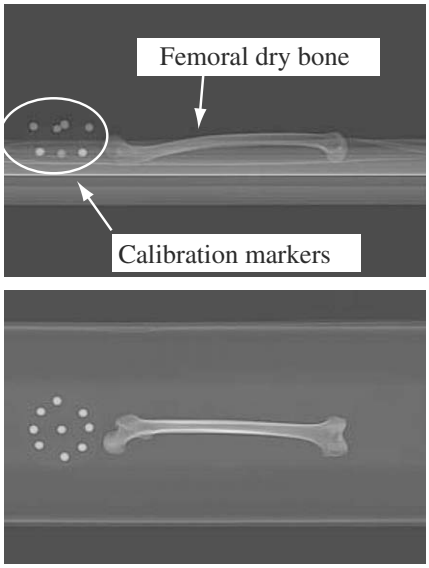

Fig. 10. Fluoroscopic images of the calibration markers and the phantom femur.

Fig. 12 shows one example of the pair (No. 4 and 24) of fluoroscopic images, which were captured from directions crossing at right angles. The average errors of the estimated femoral shape are shown in Fig. 13 and Table 2 for various numbers of shape parameters used for the estimation. The estimation process and the estimated 3D shape when the number of the estimated shape parameters is 10 are shown in Figs. 14 and 15. The calculation time by a 3.2-GHz Pentium IV, is approximately one minute, including the contour detection by the Level Set Method and the shape parameter estimation.

Finally, the average errors for various pairs of fluoroscopic images are shown in Fig. 16 when the number of the estimated shape parameters is 10. As a result of a series of experiments using the phantom femur, we concluded that the 3D shape can be estimated with an average error of less than 1.2 mm if we choose the proper images captured from directions that intersect approximately at right angles.

3.3. In vivo experiments

Next, we conducted in vivo experiments for hip prosthesis patients. Fluoroscopic images of four patients were taken in clinical practice using the fluoroscopic imaging apparatus (Siemens, Sire-

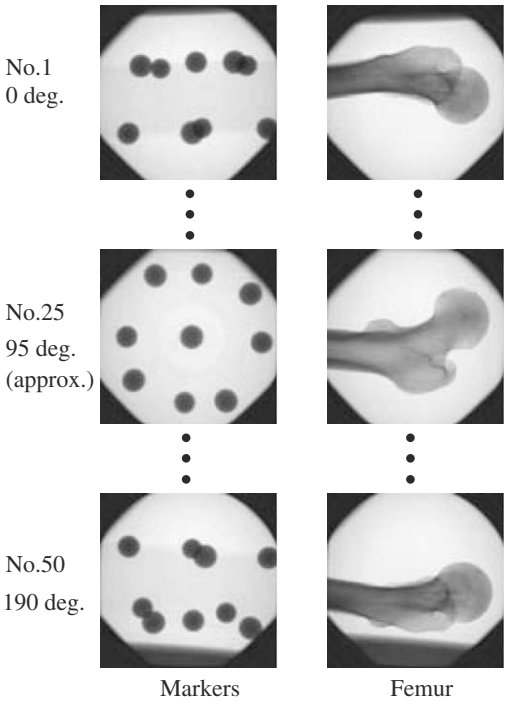

Fig. 11. Measured fluoroscopic images.

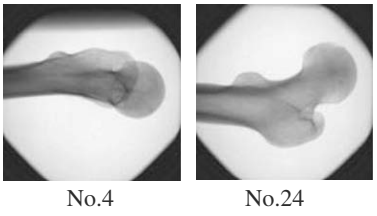

Fig. 12. Examples of fluoroscopic images (Nos. 4 and 24).

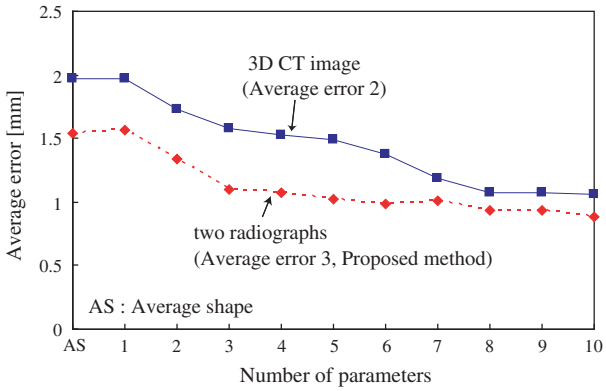

Fig. 13. Comparison of estimation errors using CT image and two radiographs.

Table 2
Average of estimation errors of the phantom femur (mm)

Number of parameters	Average	STD.	Max.
0	1.544	1.009	5.381
1	1.568	1.021	5.486
2	1.344	1.111	6.653
3	1.103	0.868	4.820
4	1.068	0.869	4.910
5	1.020	0.814	4.776
6	0.986	0.817	4.770
7	1.009	0.785	4.174
8	0.929	0.743	3.813
9	0.931	0.738	3.709
10	0.889	0.709	3.758

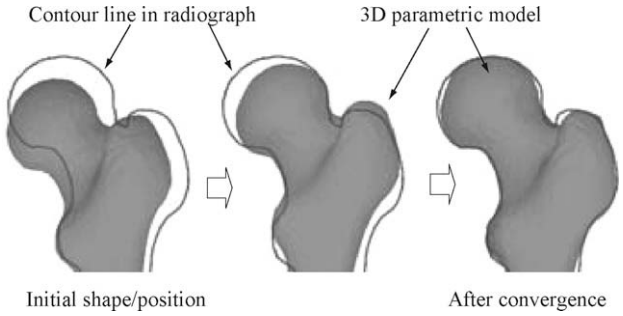

Fig. 14. Process of shape and position estimation of the femur.

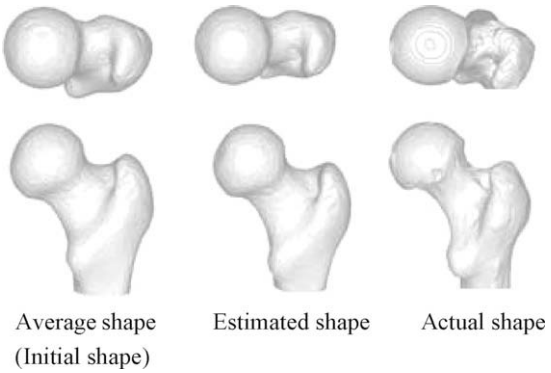

Fig. 15. Actual femoral shape and estimated femoral model with and without shape parameter estimation.

[mm]

Image No.	4	14	24	34	44
4 (≈15 deg.)		1.246	0.992	1.128	1.377
14 (≈53 deg.)	-		0.980	1.050	1.223
24 (≈91 deg.)	-	-		1.143	1.091
34 (≈129 deg.)	-	-	-		1.504
44 (≈167 deg.)	-	-	-	-	

Fig. 16. Estimation errors for various pairs of fluoroscopic images.

mobil ISO-C), and shapes measured by the CT scanner and estimated by parameter estimation were compared.

3.3.1. Calibration procedure

First, we measured the internal and external parameters of the fluoroscopic apparatus. The internal parameters consists of five parameters, that is, focus length, 1st order radial lens distortion, center pixel x and y, and scale factor. On the other hand, the external parameters contain six parameters, that is, the position and orientation of a radiation source in 3D space. After the calibration process, we can get correct fluoroscopic images of known scale without lens distortion, and the relative positions of two viewpoints. These parameters are all requisite for the proposed shape estimation procedure. A non-coplanar marker and a coplanar marker, shown in Fig. 17, are used for the calibration of external and internal parameters, respectively. These markers are constructed of acrylonitrile butadiene styrene (ABS), which indicated the highest transmission of X-rays in preliminary experimentation. The non-coplanar marker contains nine small stainless steel spheres and the coplanar marker contains 16 small stainless steel disks. The calibration procedure using these markers is as follows:

Step 1. The non-coplanar marker is captured by X-ray CT and the relative positions of the stainless steel spheres are measured.
Step 2. A fluoroscopic image of the non-coplanar marker is captured, as shown in Fig. 18, and the internal parameters of the fluoroscopic imaging apparatus are estimated by Tsai's method.
Step 3. The coplanar marker is placed under the patient's hip and two fluoroscopic images of the femur are captured from two directions, as shown in Figs. 19 and 20.

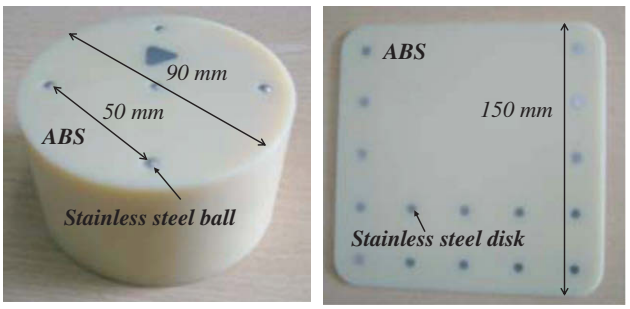

Non-coplanar marker for external parameter calibration

Coplanar marker for internal parameter calibration

Fig. 17. Non-coplanar and coplanar markers.

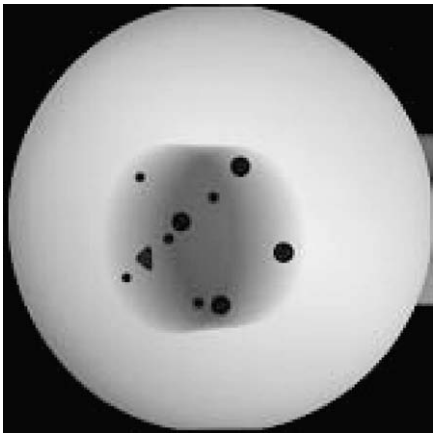

Fig. 18. Example fluoroscopic image of non-coplanar marker.

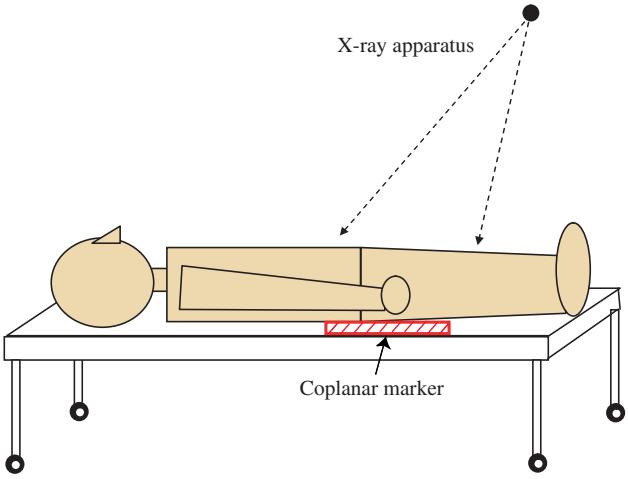

Fig. 19. X-ray photography of coplanar marker.

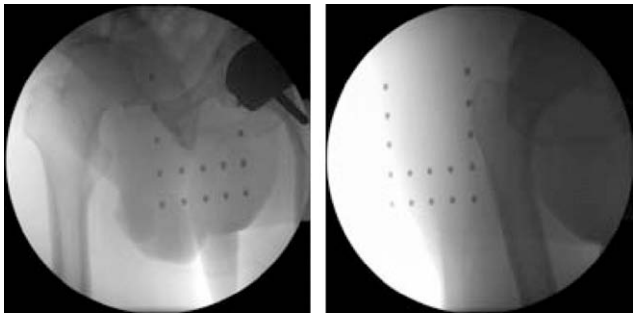

Fig. 20. Two fluoroscopic femoral images of hip prosthesis patients.

Step 4. The external parameters of two fluoroscopic images are estimated using the internal parameters obtained in Step 2 and the projection image of stainless steel disks by Tsai's method. After this calibration process, the relative positions of two viewpoints of fluoroscopic images are precisely determined.

3.3.2. Results

First, we manually extracted the contour of the femur (Fig. 21) in the fluoroscopic images (Fig. 20). Image size and resolution are 512×512 pixels and 0.454 mm pixel. We then estimated the position and 10 shape parameters from the silhouette of the femur. The precise 3D shapes of patients' femurs were measured precisely by CT scanner.

Fig. 21. Extracted contours of the femur in fluoroscopic images.

The average errors and standard deviations of the estimated femoral shapes are shown in Fig. 22. In these figures, "A" in the horizontal axis shows the case in which only the position is estimated without parameter estimation.

The experimental results show that the average error between the estimated shape and the actual shape is approximately from 0.8 to 1.1 mm for the in vivo experiments. One example of average, actual, and estimated shapes for Case 4 is shown in Fig. 23, and the distribution of average error is shown in Fig. 24. In Fig. 24, dark regions indicate less error, and the brightness of each point is proportional to its average error. From this figure, we verified that the errors in the femoral head and lesser trochanter are reduced.

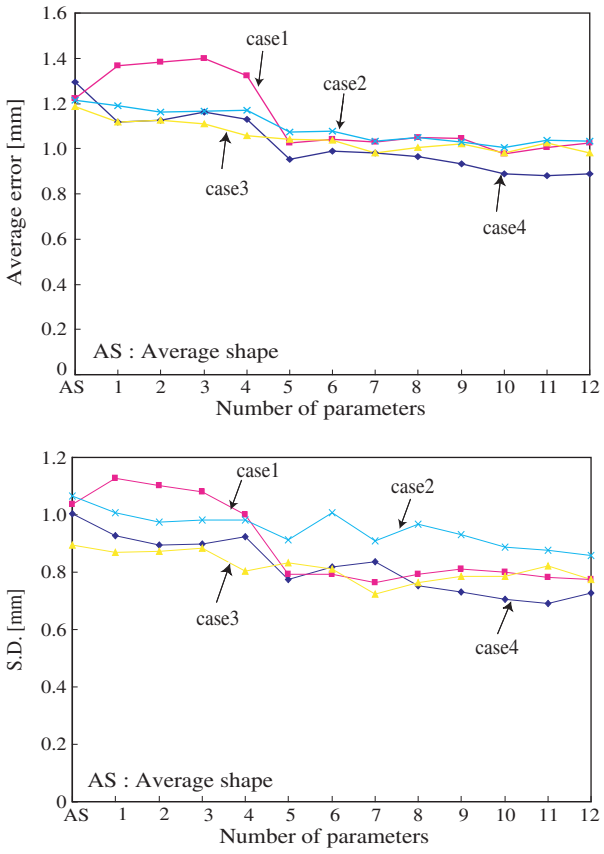

Fig. 22. Average error and standard deviation for the number of estimated shape parameters for the femurs of four patients.

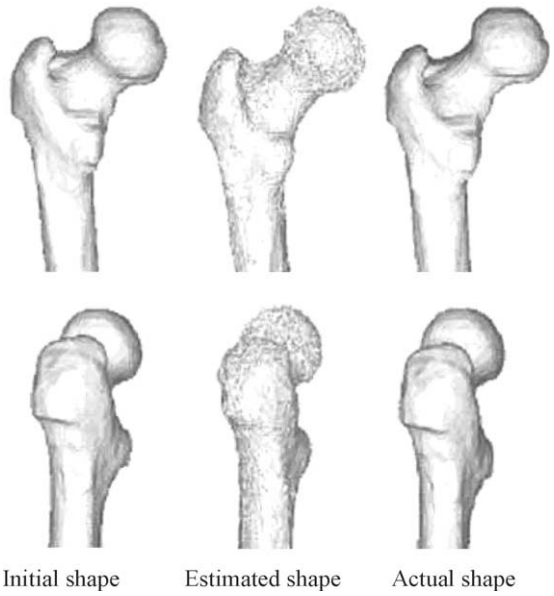

Fig. 23. Actual and estimated femoral model with and without shape parameter estimation for Case 4.

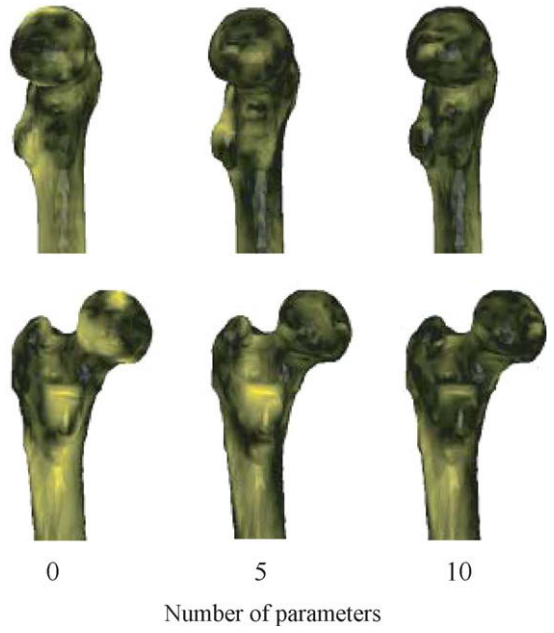

Fig. 24. Error distribution indicated by brightness (higher brightness indicates larger error.

4. Conclusions

We proposed a method by which to estimate the 3D shape of the in vivo femur from only two fluoroscopic images using a parametric femoral model. Although the precise 3D shape of the femur is usually measured using a CT scanner or an MRI system, the proposed method enables a precise 3D shape to be estimated using only two fluoroscopic images taken by an inexpensive fluoroscopic inspection apparatus. Thus, the cost of the inspection system can be dramatically reduced and the 3D image-based medical diagnosis becomes available even in small clinics.

In vivo experiments revealed the average error between the estimated shape and the actual shape to be 0.8–1.1 mm, and it was verified that the 3D shape can be estimated using two 2D fluoroscopic images taken from different view points with the same accuracy as in the case of 3D shapes being compared directly.

In the future, optimum conditions, such as the optimum number and directions of the fluoroscopic images, will be investigated, and clinical experiments in fluoroscopic image diagnosis will be performed.

Appendix A

A.1. Fast extraction of the projected contour line of the 3D parametric femoral model

In Step (4) in Section 2.3.1, the contour detection and identification triangular patches on the 3D model corresponding to points on the contour line are computationally expensive and time consuming. In our implementation, we utilize the high-speed rendering function of the OpenGL hardware accelerator, and thus these procedures are executed quite rapidly.

The detailed algorithm is as follows. Initially, we assigned different colors to all of the triangular patches in the 3D model and draw the projected image of the 3D model on the image buffer using the OpenGL hardware accelerator. The contour points of the 3D model are detected by raster scanning of the image buffer. By reading the colors of the detected contour points, we can identify the corresponding triangular patches on the 3D geometric model.

References

[1] I. Stamos, P.K. Allen, Integration of range and image sensing for photorealistic 3D modeling, in: Proceedings of the 2000 IEEE International Conference on Robotics and Automation, 2000, pp. 1435–1440.
[2] I. Stamos, P.K. Allen, Automatic registration of 2D with 3D imagery in urban environments, in: Proceedings of the International Conference on Computer Vision, 2001, pp. 731–737.
[3] L. Liu, I. Stamos, Automatic 3D to 2D registration for the photorealistic rendering of urban scenes, in: IEEE International Conference on Robotics and Automation, 2005.
[4] R. Kurazume, K. Noshino, Z. Zhang, K. Ikeuchi, Simultaneous 2D images and 3D geometric model registration for texture mapping utilizing reflectance attribute, in: Proceedings of Fifth Asian Conference on Computer Vision (ACCV), 2002, pp. 99–106.
[5] M.D. Elstrom, P.W. Smith, Stereo-based registration of multi-sensor imagery for enhanced visualization of remote environments, in: Proceedings of the 1999 IEEE International Conference on Robotics and Automation, 1999, 1948–1953.
[6] K. Umeda, G. Godin, M. Rioux, Registration of range and color images using gradient constraints and range intensity images, in: Proceedings of Seventeenth International Conference on Pattern Recognition, 2004, 12–15.
[7] Y. Iwashita, R. Kurazume, K. Hara, T. Hasegawa, Fast alignment of 3D geometrical models and 2D color images using 2D distance maps, in: Proceedings The Fifth International Conference on 3D Digital Imaging and Modeling (3DIM), 2005, pp. 164–171.
[8] Q. Delamarre, O. Faugeras, 3D articulated models and multi-view tracking with silhouettes, in: Proceedings of the International Conference on Computer Vision, vol. 2, 1999, pp. 716–721.
[9] K. Matsushita, T. Kaneko, Efficient and handy texture mapping on 3D surfaces, In Comput. Graphics Forum 18 (1999) 349–358.
[10] P.J. Neugebauer, K. Klein, Texturing 3D models of real world objects from multiple unregistered photographic views, In Comput. Graphics Forum. 18 (1999) 245–256.
[11] G. Penny, J. Weese, J. Little, P. Desmedt, D. Hill, D. Hawkes, A comparison of similarity measures for use in 2-D/3-D medical image registration, IEEE Trans. Med. Imaging 17 (4) (1998) 586–595.
[12] L. Zollei, E. Grimson, A. Norbash, W. Wells, 2D–3D rigid registration of X-ray fluoroscopy and CT images using mutual information and sparsely sampled histogram estimators, in: Proceedings of Computer Vision and Pattern Recognition, 2001, pp. 696–703.
[13] C.V. Stewart, C.L. Tsai, A. Perera, A view-based approach to registration: theory and application to vascular image regisrtaion, in: International Conference on Information Processing in Medical Imaging (IPMI), 2003, pp. 475–486.
[14] A. Guimond, A. Roche, M. Ayache, J. Meunier, Three-dimensional multimodal brain warping using the demons algorithm and adaptive intensity corrections, IEEE Trans. Med. Imaging 20 (1) (2001) 58–69.

[15] F. Maes, A. Collignon, D. Vandermeulen, G. Marchal, P. Suetens, Multimodality image registration by maximization of mutual infomation, IEEE Trans. Med. Imaging 16 (2) (1997) 187–198.
[16] C.V. Stewart, C.L. Tsai, A. Perera, Rigid and affine registration of smooth surfaces using differential properties, in: Proceedings of Third European Conference on Computer Vision (ECCV'94), 1994, pp. 397–406.
[17] C.R. Meyer, J.L. Boes, B. Kim, P.H. Bland, K.R. Zasadny, P.V. Kison, K. Korak, K.A. Fery, R.L. Wahl, Demonstration of accuracy and clinical versatility of mutual information for automatic multimodality image fusion using affine and thin plate spline warped geometric deformations, Med. Image Anal. 1 (3) (1997) 195–206.
[18] A. Gueziec, X. Pennec, N. Ayache, Medical image registration using geometric hashing, IEEE Comput. Sci. Eng. Spec. Issue Geometric Hashing 4 (4) (1997) 29–41.
[19] P.R. Andresen, M. Nielsen, Non-rigid registration by geometry constrained diffusion, Med. Image Comput. Comput. Assist. Interv. (MICCAI' 99) (1999) 533–543.
[20] T. Masuda, Y. Hirota, K. Ikeuchi, K. Nishino, Simultaneous determination of registration and deformation parameters among 3D range images, in: Fifth International Conference on 3-D Digital Imaging and Modeling, 2005, 369–376.
[21] C.S.K. Chan, D.C. Barratt, P.J. Edwards, G.P. Penney, M. Slomczykowski, T.J. Charter, D.J. Hawkes, Cadaver validation of the use of ultrasound for 3D model instantiation of bony anatomy in image guided orthopaedic surgery, in: Lecture Notes in Computer Science, 3217 (Proceedings Seventh International Conference on Medical Image Computing and Computer Assisted Intervention, Part II (MICCAI 2004), St.-Malo, France), 2004, pp. 397–404.
[22] D. Terzopoulos, D. Metaxas, Dynamic 3D models with local and global deformations: deformable superquadrics, IEEE Trans. Pattern Anal. Mach. Intell. 13 (7) (1991) 703–714.
[23] K. Nakamura, R. Kurazume, T. Okada, Y. Sato, N. Sugano, T. Hasegawa, 3D reconstruction of a femoral shape using a parametric model and two 2D radiographs, in: Proceedings of Meeting on Image Recognition and Understanding, 2006, pp. 78–83.
[24] G. Zheng, M. Ballester, M. Styner, L. Nolte, Reconstruction of patient-specific 3D bone surface from 2D calibrated fluoroscopic images and point distribution model, in: Proceedings of Medical Image Computing and Computer-Assisted Intervention (MICCAI'06), 2006, pp. 25–32.
[25] Keita Yokota, Toshiyuki Okada, Masahiko Nakamoto, Yoshinobu Sato, Masatoshi Hori, J. Masumoto, Hironobu Nakamura, Shinichi Tamura, Construction of conditional statistical atlases of the liver based on spatial normalization using surrounding structures, Int. J. Comput. Assist. Radiol. Surg. (2006) 39–40.
[26] Toshiyuki Okada, Ryuji Shimada, Yoshinobu Sato, Masatoshi Hori, Keita Yokota, Masahiko Nakamoto, Yen-Wei Chen, Hironobu Nakamura, Shinichi Tamura, Automated segmentation of the liver from 3D CT images using probabilistic atlas and multi-level statistical shape model, in: Proceedings of the Tenth International Conference on Medical Image Computing and Computer Assisted Intervention (Proc. MICCAI 2007), 2007, pp. 86–93.
[27] T.F. Cootes TF, C.J. Cooper, C.J. Taylor, J. Graham, Active shape models—their training and application, Comput. Vis. Image Understanding 61 (1) (1995) 38–59.
[28] T. Okada, M. Nakamoto, Y. Sato, N. Sugano, H. Yoshikawa, S. Tamura, T. Asaka, Y.-W. Chen, Effects of surface correspondence methods in statistical shape modelling of the proximal femur on approximation accuracy, in: Proceedings of the Twenth International Congress and Exhibition Computer Assisted Radiology and Surgery CARS, 2006, p. 016.
[29] Haili Chui, Anand Rangarajan, A new point matching algorithm for non-rigid registration, Comput. Vis. Image Understanding 89 (2-3) (2003) 114–141.
[30] M. Greenspan, M. Yurick, Approximate k-d tree search for efficient ICP, in: Proceedings of 3-D Digital Imaging and Modeling 3DIM, 2003, pp. 442–448.
[31] J. Sethian, Level Set Methods and Fast Marching Methods, second ed., Cambridge University Press, UK, 1999.
[32] J. Sethian, A fast marching level set method for monotonically advancing fronts, in: Proceedings of the National Academy of Science 93, 1996, pp. 1591–1595.
[33] G. Borgefors, Distance transformations in arbitrary dimensions, Comput. Vis. Graphics Image Process. 27 (3) (1984) 321–345.
[34] S.W. Shih, Y.T. Wu, Fast Euclidean distance transformation in two scans using a 3 3 neighborhood, Comput. Vis. Image Understanding 93 (2) (2004) 195–205.
[35] R.Y. Tsai, An Efficient and Accurate Camera Calibration Technique for 3D Machine Vision, in: Proceedings of IEEE Conference on Computer Vision and Pattern Recognition, 1986, pp. 364–374.